A&A 403, 83–91 (2003)
DOI: 10.1051/0004-6361:20030375

Astronomy & Astrophysics

Clumps in large scale relativistic jets

F. Tavecchio[1], G. Ghisellini[1], and A. Celotti[2]

[1] INAF, Osserv. Astron. di Brera, via Bianchi 46, 23807 Merate, Italy
[2] SISSA/ISAS, via Beirut 2-4, 34014 Trieste, Italy

Received 9 December 2002 / Accepted 25 February 2003

Abstract. We estimate the time dependent emission of the bright knots detected in large scale (tens to hundreds kpc) jets and discuss how the existing radio–to–X–ray observations, coupled with the correspondingly long cooling timescales, pose strong constraints on the structure and dynamics of knots. We suggest that the phenomenology of the jet in 3C 273 as observed by HST, Chandra and VLA, and in particular the fast decrease of the flux outside knots, can be satisfactorily accounted for if the emitting plasma is clumped. Clumping of the knots can also explain the month–year variability timescale reported for the large scale emission in M 87. We also point out that emission between the bright knots should be detected with the next generation of instruments (e.g. NGST). In fact the relatively intense X–ray emission discovered with Chandra suggests that jets (at least in powerful quasars) are still relativistic at large distances from the active nucleus. In such a case Compton scattering off the CMB photons is efficient even when electrons are cold or mildly relativistic in the comoving frame. This provides a powerful tool for testing the continuous vs discrete nature of the jet flow.

Key words. galaxies: jets – galaxies: nuclei – radio continuum: galaxies

1. Introduction

Chandra observations revealed X–ray emission from knots in jets of extragalactic radio sources at distances of tens to hundreds kpc from the nucleus. This occurs both in powerful flat spectrum radio sources (FSRQ) whose jet is probably aligned with the line of sight (Chartas et al. 2000; Pesce et al. 2001; Sambruna et al. 2002; Sambruna et al. 2001; Schwartz 2002; Schwartz et al. 2000; Siemiginowska et al. 2002; Tavecchio et al. 2000), and in closer radio galaxies whose jets are instead observed at large viewing angles (e.g. Wilson & Yang 2002; Kraft et al. 2002; Hardcastle et al. 2002; Hardcastle et al. 2001; Wilson et al. 2001).

In powerful FSRQ the X–ray luminosity often exceeds the optical and radio powers emitted in the same knot. Thermal and synchrotron self-Compton emission models have difficulties in explaining the data (see e.g. Chartas et al. 2000; Schwartz et al. 2000; Siemiginowska et al. 2002; Harris & Krawczynski 2002), while interpreting the X–rays as due to inverse Compton (IC) off the cosmic microwave background (CMB) photons and the radio–optical emission as due to synchrotron radiation, satisfactorily accounts for the observations and at the same time minimizes the energy requirements (Celotti et al. 2001; Tavecchio et al. 2000; Ghisellini & Celotti 2001). This however requires jets to be highly relativistic even at the largest scales: in the case of PKS 0637–712 the bulk Lorentz factor Γ should be of the order of 10–15 hundreds kpc away from the core. Bulk relativistic motion in fact implies that the CMB energy density is seen boosted by a factor $\sim\Gamma^2$ in the plasma comoving frame, and therefore can dominate over the local synchrotron and magnetic energy densities.

Another consequence of this scenario is that the low energy end of the emitting particle distribution, $\gamma_{\rm min} m_{\rm e} c^2$, is tightly constrained. For example in the case of PKS 0637–752 it is required that $\gamma_{\rm min} < 30$ for the inverse Compton process to produce photons with energies in the softest X–ray band (assuming $\Gamma = 14$), and $\gamma_{\rm min} > 10$ to avoid the inverse Compton process to overproduce the observed optical emission. This latter constrain holds independently of whether the optical emission is due to low energy inverse Compton photons or to the high energy tail of the synchrotron component. A synchrotron origin of the optical radiation implies – for reasonable values of the magnetic field – the presence of electrons of TeV energies. These have relatively short cooling timescales nicely accounting (albeit within the large uncertainties) for the dimensions of the optical knots as observed by HST (Schwartz et al. 2000; Celotti et al. 2001).

However at these scales the electron cooling time is relatively long for all but the highest energy particles. Therefore it is meaningful to estimate the spectral energy distribution (SED) of emission *outside* the bright knots. And indeed available observations pose an interesting problem in this respect: outside the bright knots the X–ray flux is dimming as fast as the optical and radio fluxes, despite of the fact that it should

Send offprint requests to: F. Tavecchio,
e-mail: tavecchio@merate.mi.astro.it

be produced by low energy electrons, which do not cool radiatively. Adiabatic losses could account for such a behavior, but the requirement on the source expansion rate implies interesting conclusions about the structure of the acceleration sites. The main result of our analysis is that if a knot is homogeneously filled by a single relativistic particle population radiative and adiabatic losses alone cannot account for the fast decrease of the emission outside it. We discuss possible solutions to this problem and finally propose a scenario that seems to account for the main properties of the knot emission.

The issue of the slow cooling of particles on such jet scales is also discussed in relation to the intriguing possibility – potentially a powerful jet diagnostic – of detecting inverse Compton radiation produced by particles that are only mildly relativistic or even sub-relativistic in the comoving frame but have substantial bulk motion. In fact on one hand the magnetic field likely decreases with increasing distance from the nucleus, causing the synchrotron luminosity to decrease even if the emitting particles do not cool. On the other hand for a non-decelerating jet the CMB energy density is constant (in the comoving frame) and therefore the inverse Compton scattering of these photons is always effective. Such "bulk Compton" luminosity, expected also from particles present between bright knots if the jet is a continuous fluid, might indeed be observable by existing or future instruments, such as ALMA and NGST.

In order to tackle these issues we first compute the time evolution of an emitting particle distribution. In the presence of bulk motion, the time evolution translates into a spatial profile from the acceleration site. However, this correspondence is not unique, since it depends on the nature of the bright knots, and in particular on whether they correspond to *stationary* or *moving* features. In the former case relativistic particles accelerated at a shock propagate away from it, forming a trail; in the latter case there is no close connection between the bright knots (which are moving with the emitting particles) and the inter-knot regions.

The outline of the paper is the following. The evolution of a particle distribution subject to radiative and adiabatic cooling is presented in Sect. 2. This is compared with available observations in Sect. 3 and in Sect. 4 a possible scenario accounting for the discrepancies between the predictions and the observations is presented. Section 5 summarizes the results which are discussed in Sect. 6.

2. Adiabatic and radiative losses

In this section we compute the evolution of a distribution of relativistic particles subject to both radiative and adiabatic cooling and apply the results to the overall knot emission.

2.1. The evolution of the electron distribution

Let us define $N(\gamma, r)$ as the particle energy distribution at some distance r from an initial site r_0, where N represents the total number of electrons (not the density). The plasma is assumed to have bulk motion with velocity βc and Lorentz factor Γ. In the absence of (re)–acceleration, the evolution of $N(\gamma, r)$ is described by (e.g. Sikora et al. 2001)

$$\frac{\partial N}{\partial r} = \frac{\partial}{\partial \gamma}\left(N \frac{\mathrm{d}\gamma}{\mathrm{d}r}\right). \quad (1)$$

This is the usual continuity equation in which time has been substituted by the radial coordinate r through $r = \beta c \Gamma t'$, and t' is the time measured in the comoving frame. As our results will concern powerful FSRQ, we assume that inverse Compton losses (off CMB photons) dominate over synchrotron losses, i.e.

$$\frac{\mathrm{d}\gamma}{\mathrm{d}r} = -\frac{1}{\beta c \Gamma} \frac{4\sigma_T c U_{\rm rad}}{3 m_{\rm e} c^2} \gamma^2 - A\frac{\gamma}{r}, \quad (2)$$

where $U_{\rm rad} = 4 \times 10^{-12}(1+z)^4 \Gamma^2$ erg cm^{-3} and the latter term represents adiabatic cooling: $A = 1$ for 3D expansion and $A = 2/3$ for 2D expansion. The solution of Eq. (2) is

$$\gamma = \frac{(1-A)}{\alpha\, r + (r_0/r)^{-A}[(1-A)/\gamma_0 - \alpha\, r_0]} \quad (3)$$

where $\alpha \equiv 4\sigma_T U_{\rm rad}/(3\beta\Gamma m_{\rm e} c^2)$. All particles with initial energies between γ_0 and $\gamma_0 + \mathrm{d}\gamma_0$, in a time t (or after some distance r), have energies between γ and $\gamma + \mathrm{d}\gamma$, where γ is given by Eq. (3). From Eq. (3) we thus have:

$$\frac{\mathrm{d}\gamma}{\mathrm{d}\gamma_0} = \frac{(1-A)^2}{\gamma_0^2 (r_0/r)^A}\left[\alpha\, r + \left(\frac{r}{r_0}\right)^A \left(\frac{1-A}{\gamma_0} - \alpha\, r_0\right)\right]^{-2}. \quad (4)$$

Therefore the particle distribution at a given distance r and energy γ is obtained by calculating the corresponding initial γ_0 (cooled to γ in the time to move from r_0 to r) and taking into account the corresponding differentials:

$$N(\gamma, r) = \frac{N_0(\gamma_0, r_0)}{\mathrm{d}\gamma/\mathrm{d}\gamma_0}. \quad (5)$$

Figure 1 shows an example of particle evolution calculated according to Eq. (5). Note that the total number of particles is conserved: since the low energy cutoff moves to lower energies (because of adiabatic losses), the normalization decreases with r.

2.2. Results

We have computed the evolution of the SED as a function of r (Eq. (5)), assuming a power law distribution $N(\gamma_0, r_0)$ between $\gamma_{\rm min,0}$ and $\gamma_{\rm max,0}$. The initial parameters, listed in Table 1, have been chosen to roughly match those required to fit the SED of a typical large scale knot visible in the radio, optical and X–ray bands. The magnetic field is assumed to scale as r^{-1} (as in the case the field has a dominant toroidal component or in the case of constant magnetic flux along the jet). Note that the intensity of the magnetic field does not affect the particle evolution (since we have assumed that IC on the the CMB radiation dominates the cooling), but it determines the amount of emitted synchrotron radiation. We have also assumed that the total number of electrons in a "slice" of the jet of width Δr is conserved, and that Δr is constant. An adiabatic constant $A = 2/3$, corresponding to 2D expansion, has been consistently set.

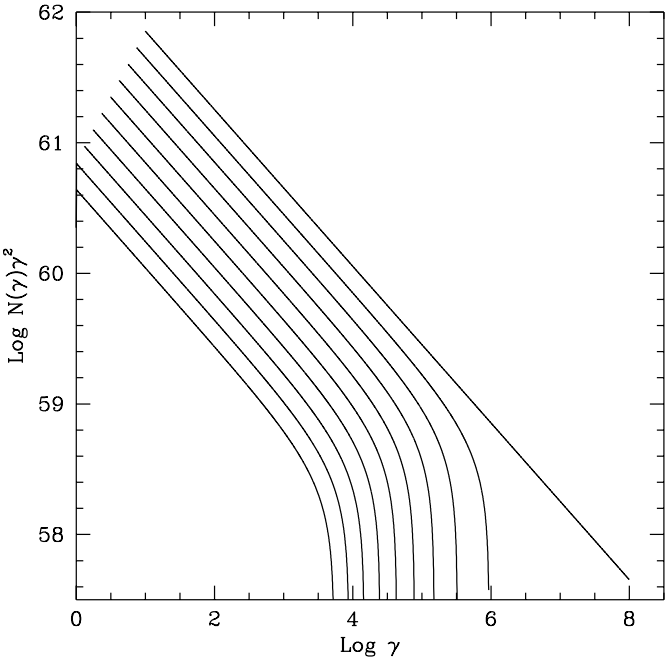

Fig. 1. The evolution of the particle distribution with r, calculated assuming an initial power-law distribution and the parameters listed in Table 1. Note that $\gamma_{\rm min}$ decreases with r due to adiabatic losses. As the total particle number is conserved the normalization also decreases with r.

Table 1. Input parameters for the cases illustrated in Figs. 1–9. For all of them we assumed $r_{\rm max} = 50 r_0$ and $N(\gamma_0, r_0) \propto \gamma_0^{-n}$ with $n = 2.6$.

r_0 kpc	B_0 μG	A	$\gamma_{\rm min,0}$	$\gamma_{\rm max,0}$	Γ	δ	z	Fig.
20	36	2/3	10	1e8	15	5.4	0.72	1
20	36	2/3	10	2.4e5	4	6	1	2, 3
20	36	2/3	10	5e5	4	6	1	4
20	10	2/3	10	2.4e5	15	9	1	5, 6
20	10	2/3	10	5e5	15	9	1	7
0.16	10	1	20	1e6	15	15	1	8, 9

We have estimated not only the SED but also the flux profiles at different frequencies. Different possibilities have been explored. Jets with bulk Lorentz factors $\Gamma = 4$ and $\Gamma = 15$ have been considered, since this is the range of values found from fitting the SED of large scale X–ray structures of quasars (Tavecchio et al. 2000; Celotti et al. 2001; Sambruna et al. 2002). Furthermore the calculations have been performed both in the case the optical flux is due to the low energy tail of the IC component (SEDs in Figs. 2 and 5, profiles in Figs. 3 and 6) and in the case it constitutes the high energy emission of the synchrotron component (profiles shown in Figs. 4 and 7). The only input parameter changing between these two situations is the value of $\gamma_{\rm max,0}$.

Let us examine the results. In Fig. 2 we show the SEDs computed (for $\Gamma = 4$) in the assumption that the optical emission, at the starting point r_0, is due to the lower energy photons produced by the IC scattering off the CMB. Therefore the electrons mostly producing this radiation have low energies and

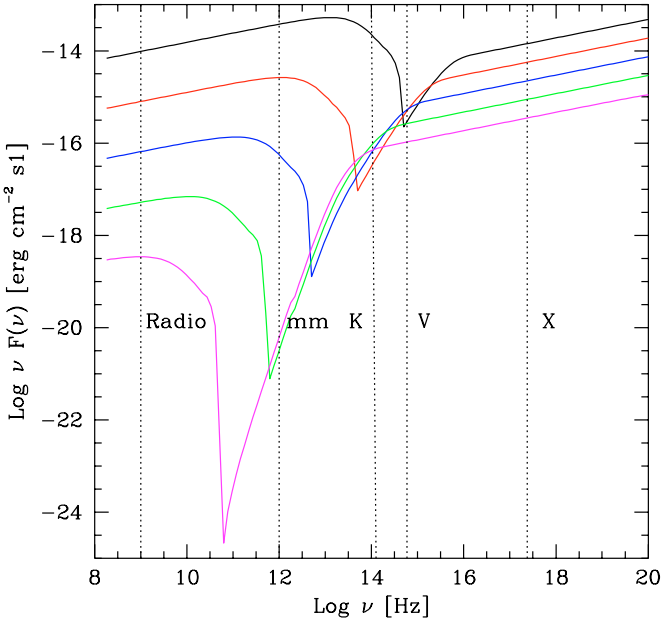

Fig. 2. SEDs calculated according to the parameters listed in Table 1. From top to bottom: r = 20, 53, 140, 370 and 980 kpc. $\Gamma = 4$ is assumed.

their cooling time is long. The IC emission dominates the bolometric luminosity but not by a large factor at the beginning (the IC component also dominates at early times, although this may not be immediately clear from Fig. 2 in which the IC spectrum is cut before its peak). At later times (or at larger distances from r_0) the Compton dominance increases, since the magnetic field decreases as r^{-1} while the energy density of the CMB is constant. Figure 3 illustrates the corresponding expected profiles of the flux in different bands using the same parameters as in Fig. 2 (and listed in Table 1). The x–axis of the figure can represent the distance from the starting point (bottom axis) or equivalently the time elapsed since the injection of $N(\gamma_0, r_0)$ (top axis). In the latter case the light curves shown do not take into account light travel time effects: since the source is very extended, at any time light from different evolutionary phases of the source contributes to the observed flux. This effect is important of course for $t < r_0/c$: at these times the observed light curve is not represented by that shown in Fig. 3 (and the analogous Figs. 4, 6 and 7), but should be calculated by considering the different travel paths of light rays produced in different parts of the source (see e.g. Chiaberge & Ghisellini 1999). For the aims of this work these effects are not crucial, but they will be properly considered in our future studies. Note however that if the profiles (i.e. bottom x–axis) correspond to emission from a standing shock (see below), then light travel time effects are not important, and Fig. 3 (and the other analogous figures) already appropriately describes the expected behavior.

The profiles in the case of optical emission due to the high–energy tail of the synchrotron component are shown in Fig. 4. The only parameter different from those adopted for Figs. 2 and 3 is a slightly lower $\gamma_{\rm max,0}$ (see Table 1). Clearly the main difference with respect to the previous situation is a fast initial decrease of the optical flux.

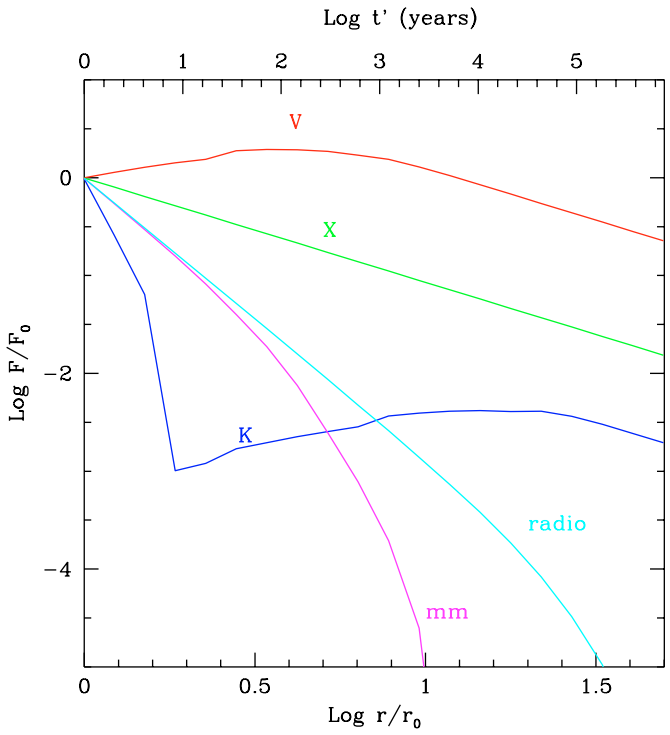

Fig. 3. Flux profiles at different frequencies (5 GHz, 0.2 mm, *K* band, *V* band and 1 keV), calculated assuming the parameters listed in Table 1. $\Gamma = 4$ is assumed. In the conditions considered the optical emission is due to inverse Compton off the CMB photons. The optical *initially increases* moving away from the knot in case A (bottom *x*–axis) or initially increases in time in case B (top *x*–axis, time is measured in the knot's frame). See text for details on the two cases. The initial values of the fluxes at the different frequencies are: $F_{5\ \rm GHz} = 209$ mJy, $F_{0.2\ \rm mm} = 4$ mJy, $F_K = 20\ \mu$Jy, $F_V = 0.1\ \mu$Jy, $F_{1\ \rm keV} = 6.2$ nJy.

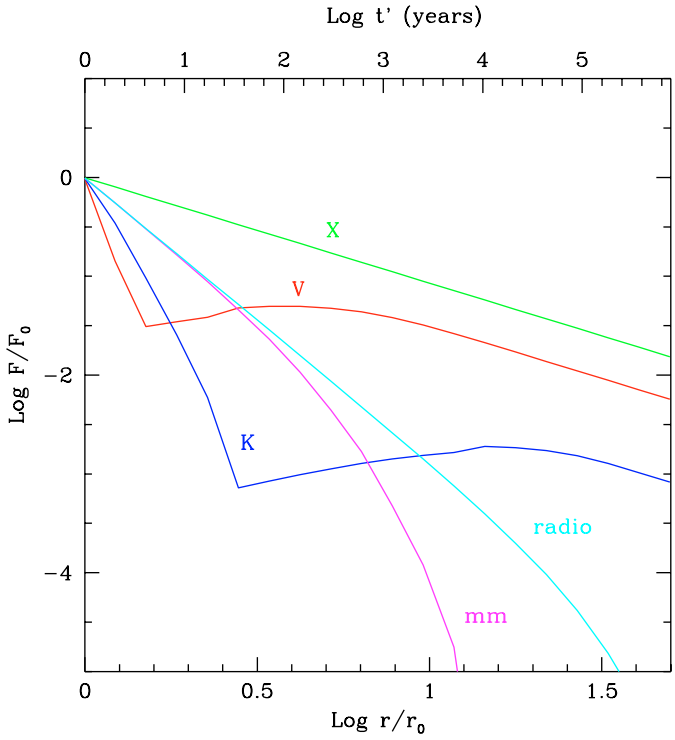

Fig. 4. Flux profiles at different frequencies, assuming the parameters reported in Table 1, for $\Gamma = 4$. In this case the optical emission is produced as synchrotron radiation. The initial values of the fluxes at the different frequencies are the same as in Fig. 3, except for the optical flux, here $F_V = 2\ \mu$Jy.

By contrast Fig. 5 shows the SEDs predicted for $\Gamma = 15$. In this case the inverse Compton emission is more dominant than in the previous case, due to the increased energy density of the CMB as seen in the comoving frame ($\propto \Gamma^2$). The other input parameters are listed in Table 1. Note that because of the higher comoving CMB energy density, the radiative cooling times are shorter than in the $\Gamma = 4$ case, making the evolution of the high energy electrons faster, as shown by the comparison of the radio and far IR emission in Figs. 5 and 2 at late times (or large distances). As in Fig. 2, the SEDs presented in Fig. 5 correspond to the case of optical emission produced by the inverse Compton process. Note that the flux between the synchrotron and IC components becomes negligible at late times, when only the low energy electrons still radiate. Figure 6 shows the corresponding flux profiles at different frequencies, while Fig. 7 illustrates the profiles assuming that initially the optical flux is due to the tail of the synchrotron component.

The flux profiles reveal a general trend, namely that the synchrotron emission is dimming faster than the IC one, due to: i) the different electron energies involved and ii) the decreasing magnetic field. In all cases the X–ray fluxes are approximately linearly decreasing with the distance *r*, while the initial decrease of the synchrotron emission (away from the spectral cutoffs) scales roughly as r^{-3}. As discussed below, this different behavior is crucial when comparing our results with existing data.

2.3. Interpretation of the results

As mentioned in the Introduction, there are different possible frames for interpreting the results presented in Figs. 3, 4 and Figs. 6, 7. Assuming that a shock is responsible for the acceleration of the emitting particles, different cases can be identified through the velocity of the shock front relative to the bulk velocity of the downstream emitting plasma. In the following we consider, for simplicity, the two more extreme cases:

case A: streaming of particles from a stationary shock (corresponding to the bottom *x*–axis, i.e. the distance from the acceleration site);

case B: moving blob in which particles have been accelerated (corresponding to the top *x*–axis, i.e. the time from the acceleration event in the blob reference frame).

In case A, Figs. 3, 4, 6 and 7 show the profiles that would be observed in deep images of jets for $r > r_0$ (assuming that the shock lifetime allows particles to propagate from r_0 to *r*). If the optical emission is due to the low–energy tail of the IC component (Figs. 3 and 6) the optical flux *increases* with *r*. In fact, despite of the decrease in the normalization of $N(\gamma)$, $\gamma_{\rm min}$ decreases, i.e. the overall spectrum shifts to lower frequencies, and thus at low energies the flux increases.

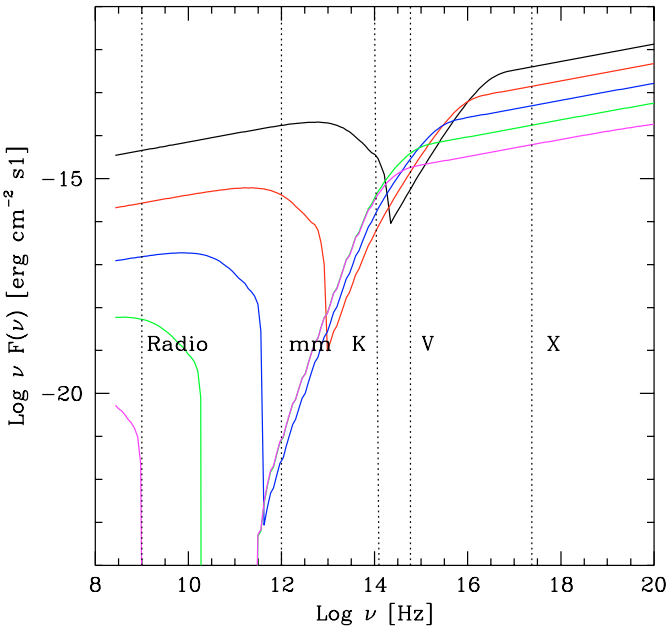

Fig. 5. SEDs calculated according to the parameters listed in Table 1. From top to bottom: r = 20, 53, 140, 370 and 980 kpc. Γ = 15 is assumed.

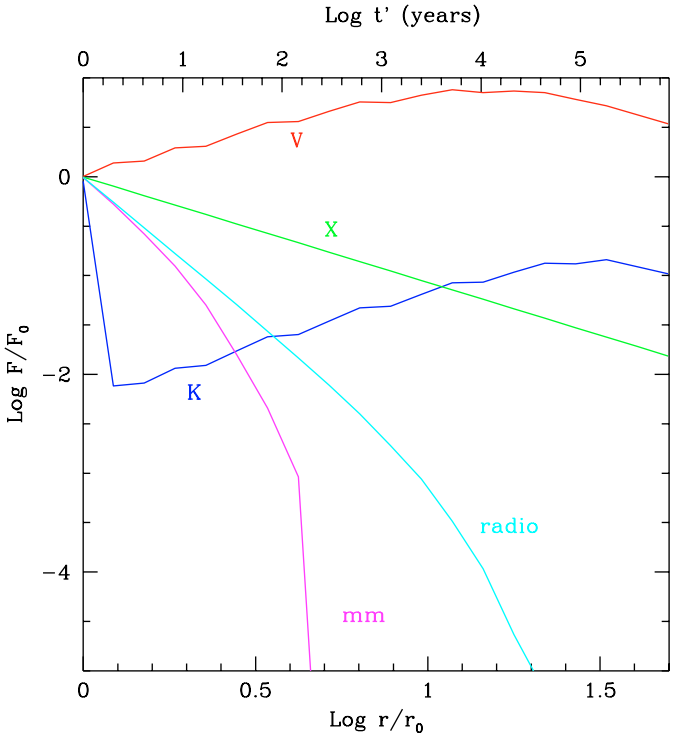

Fig. 6. Flux profiles at different frequencies (5 GHz, 0.2 mm, K band, V band and 1 keV), for Γ = 15, calculated assuming the parameters listed in Table 1. The optical emission is due to IC off the CMB radiation field. Also in this case (as in Fig. 3) the optical initially increases moving away from the knot in case A (bottom x–axis) or initially increases in time in case B (top x–axis, time is measured in the knot's frame). See text for details on the two cases. The initial values of the fluxes at the different frequencies are: $F_{5\ \mathrm{GHz}}$ = 93 mJy, $F_{0.2\ \mathrm{mm}}$ = 1.7 mJy, F_K = 3 μJy, F_V = 0.13 μJy, $F_{1\ \mathrm{keV}}$ = 208 nJy.

In case B, the particle distribution at a given r is not directly related to the detected bright knots, but is instead the "fossil" distribution of acceleration phases occurred in the past (at $t' = t'_0$, top x–axis). If such phases occurred with the optical flux initially produced through IC, some bright optical knots with relatively weak X–ray and radio fluxes (with respect to those detected by HST/Chandra) should be observable. As knots bright only in the optical band have not been detected, this could imply that the optical emission is always due to the high energy tail of the synchrotron spectra, i.e. to high energy electrons. However, as discussed below, an alternative possibility is that the knot emission is due to the contribution of many emission sites, with sub-knot dimensions.

3. Comparison with observations

The results of the analysis described above can be compared with the observed profiles of nearby jets. Here we concentrate on the case of the luminous jet of 3C 273, one of the sources with the best quality data currently available (Sambruna et al. 2001; Marshall et al. 2001)

The jet presents numerous knots visible in radio, optical and X–rays. The analysis of the data by two groups (Sambruna et al. 2001; Marshall et al. 2001) leads them to different conclusions about the viability of a synchrotron interpretation for the X–ray emission in knots A and B1 (the two most luminous portions of the jet). This discrepancy is due to the different optical spectral slopes derived by the two teams. As Sambruna et al. (2001) infer a slope systematically steeper than that of Marshall et al. (2001), they can rule out the possibility that a unique spectral component can account for the overall radio to X–ray spectrum, while the opposite conclusion is preferred by Marshall et al.

Despite this disagreement, both groups attribute the optical flux to synchrotron emission and find that maps at different frequencies yield the same knot dimensions and similar flux profiles. In other words, it appears there is no frequency dependence of the knot sizes. However, according to our analysis, radio knots would be expected to be larger than the optical ones, due to the longer lifetime of the radio emitting electrons. An even larger size would be predicted for the X–ray knots if produced by the IC process (i.e. by very low energy electrons).

In the following we examine possible and most plausible explanations for the discrepancy between observations and our expectations. These invoke adiabatic losses as a more efficient coolant than radiative losses for the low energy electrons.

– Consider an unresolved standing shock, namely a compact acceleration site, typically smaller than the Chandra resolution of about one arcsec. This corresponds to a region (r_0 in our models) which is less than a kpc in size (say a factor 10 smaller). Because of the small dimension the doubling timescales are short enough for adiabatic losses to be effective in decreasing the flux. *However, such a possibility is excluded by the HST observations which in fact resolve the optical emission region on scales of about 1 arcsec.* This implies that the acceleration site either exceeds 1 arcsec in size or is made up by several sub–units.

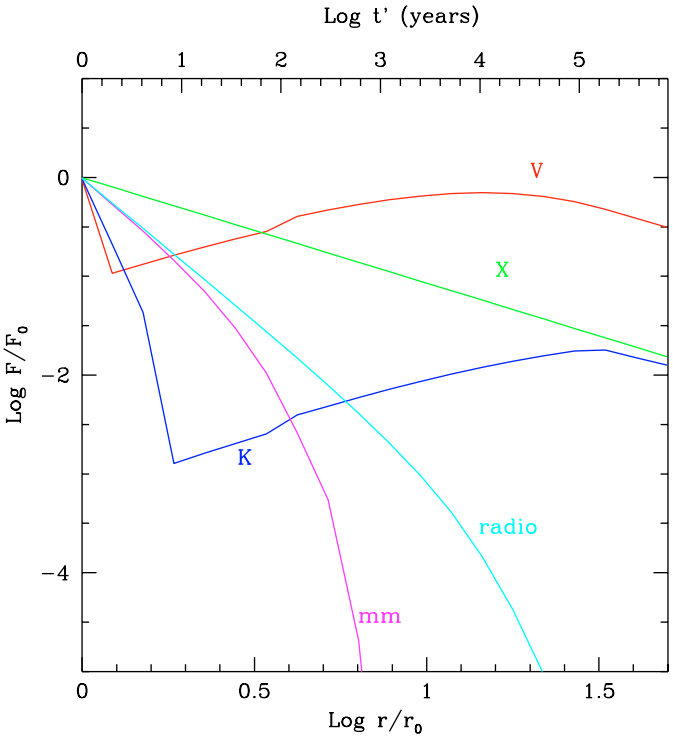

Fig. 7. Flux profiles at different frequencies, for $\Gamma = 15$, assuming the parameters reported in Table 1. The optical radiation is due to synchrotron. The initial values of the fluxes at the different frequencies are the same as in Fig. 6 except for the optical flux, here being $F_V = 1.5\,\mu$Jy.

– Let us discuss the scenario in which the emission regions can be approximated as moving blobs. In such a case the observed knots correspond to a snapshot of the currently active blobs. Thus the emission at different frequencies can be cospatial with no emission between knots. As knots are simultaneously active according to the observing time, due to the different light travel times they have been "lighted up" at different intrinsic times. This however requires fine tuning if these knots were the only sites of dissipation. If instead more blobs than observed are present and randomly (in time and location) light up, there is the possibility of always observing a few of them active. This requires the existence of "fossils" of previous active phases, emitting some X–rays, radio, and no optical (i.e. only low energy electrons still emitting). But this is contrary to the lack of observed "fossil" knots. Yet another alternative is to assume that only a few blobs exist and are *always* active. In this case no fossil emission is expected, but particles in each knot have to be continuously re-accelerated. However this leads to another problem: if the same particles are continuously re-accelerated they should reach a typical energy (at which the cooling and acceleration timescales are comparable) causing a pile–up in the particle distribution at some energy, which is not observed. A possible way out is to assume that particles are only episodically re-accelerated, but this would also require a fine tuning between the duty cycle of the acceleration episodes and the cooling time of the optical electrons (as the two timescales would have to be comparable).

We conclude that simple alternatives to the scenario of a single homogeneous region emitting by synchrotron and external Compton are not satisfactory or require fine tuning. We therefore explore a slightly more complex possibility, namely the situation of clumped knots.

4. The clumping scenario

The key point of assuming that knots are not homogeneous, but clumped (i.e. formed by several smaller sub-structures which may be identified with acceleration sites) is that the clumps can expand faster than the entire knot and therefore adiabatic losses can be more effective.

Let us consider N clumps/acceleration sites much smaller than the transverse dimension of the jet and for simplicity all with the same physical properties, i.e. characterized by the same particle density n_i, size R_i, volume V_i and bulk Lorentz factor Γ_i. The corresponding filling factor is $f \equiv NV_i/V$ where V is the volume of the entire knot and R_i is limited to be typically smaller than one tenth of the knot size for the expansion losses to be sufficiently efficient. Just for illustrative purposes, let us then compare the predictions of the case of a single homogeneous region (the one–zone scenario discussed in the literature) with those of the clumped case. For simplicity the total number of emitting particles as well as the bulk Lorentz factor are assumed to be the same in the two situations. With these assumptions the magnetic field B_i has to be similar to that in the case of a homogeneous knot, independently of R_i and N. This is because, with the same Lorentz factor, the radiation energy density $U_{\rm rad}$ is the same in both scenarios. Then, in order to mantain the same synchrotron over inverse Compton luminosity ratio, also the magnetic field energy density must be the same. The size of the clumps then uniquely determines the density n_i, which is a factor f^{-1} larger than in the one–zone case.

Note that within these assumptions the average bulk kinetic power is dominated by the cold proton component (assuming one proton per electron) and is also the same in the two scenarios, as it is determined by the total particle number and the flow velocity.

There is no obvious lower limit to the clump size R_i, but it should be noted that (within our assumptions) for any fixed number of clumps the smaller is R_i, the larger n_i, and thus the larger the deviation from equipartition between particle and magnetic energy densities. This deviation scales as the ratio of the particle density in each clump and that in the one–zone case, i.e. as f^{-1}. Therefore many small clumps imply a large deviation from equipartition.

In conclusion, we propose that knots are actually constituted by clumps which are the sites of particle acceleration, and which are denser and hotter than the surroundings. Because of the enhanced particle pressure with respect to the one–zone case, the clumps are likely to be overpressured with respect to their surroundings, implying expansion. The observed

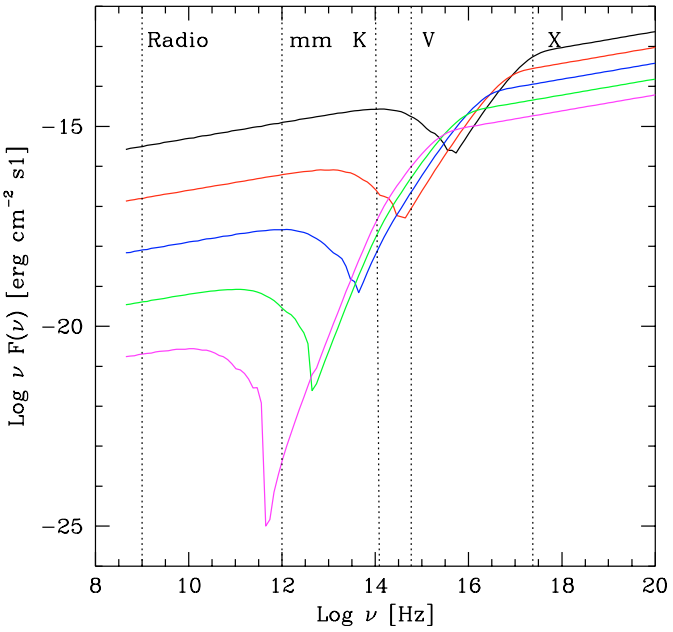

Fig. 8. SEDs calculated in the clumped knot scenario, adopting the parameters listed in Table 1. The figure illustrates the spectral evolution of a single clump at different expansion stages. From top to bottom: $r = 0.16$, 0.28, 0.5, 0.9 and 1.6 kpc. Note that for this case we assume a 3D expansion and correspondingly $A = 1$.

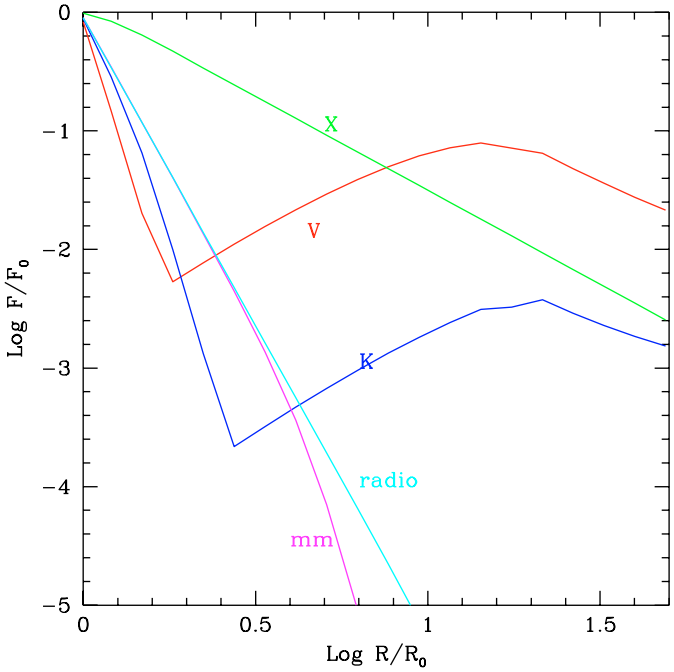

Fig. 9. Flux profiles at different frequencies (5 GHz, 0.2 mm, *K* band, *V* band and 1 keV), for $\Gamma = 15$, in the case of a single clump, for the same parameters as in Fig. 8.

emission would be the convolution of the radiation produced by such expanding clumps.

The understanding of the formation process(es) of the clumps is beyond the aims of this work and we only mention as possible candidates instabilities, clouds (filaments) crossing the jet (as proposed by e.g. Blandford & Königl 1979 in relation to jets on smaller scales), or instabilities triggered by entrained gas that can act as an obstacle for the flow, leading to formation of shocks. Another possibility is that particle acceleration is induced by reconnection events (e.g. Drenkhahn & Spruit 2002) and in this case the clumps could be identified with the reconnection sites.

If such clumps do exist, then low energy electrons can adiabatically cool before they reach the size of the knot detected by Chandra, and the problem outlined above can be solved. To illustrate this, we show in Figs. 8 and 9 respectively the SEDs and the corresponding flux profiles at different frequencies for a single clump. As expected, since r_0 is smaller than in the previous cases, the adiabatic timescales are shorter, changing the relative importance of the radiative and adiabatic losses. Note that the entire range of the *x*–axis of Fig. 9 is now 1 arcsec, as opposed to 10 arcsec of the previous cases (for a source at $z \sim 1$).

If electrons can propagate away from the acceleration sites while cooling for radiative and adiabatic losses, the emit some radiation also outside the clumps. As the high energy particles, producing the optical synchrotron radiation, cool more rapidly the optical flux decreases initially at the faster rate. When $\gamma_{\rm min}$ is low enough to radiate in the optical via inverse Compton off the CMB photons, the optical flux increases (as long as it corresponds to the rising tail of the IC spectrum). The same situation occurs (but at later times) for the infrared flux. The X–ray emission, always produced by low energy electrons, instead steadily decreases. Then the prediction of this scenario is that each clump should be resolved with high enough angular resolution, especially in the optical and infrared bands, for which the contrast between the emission inside and outside the clumps is the largest. The flux between clumps remains at a considerable level chiefly in the X–ray band. Crucial observations in this respect would require sub–arcsec angular resolution at flux levels of the order of 10^{-15} erg cm^{-2} s^{-1} or better, at least in the optical/IR and possibly in the mm and radio domains. These capabilities are in the reach of NGST, LBT and ALMA.

5. Summary

We have discussed how the presence of low energy electrons in jets, predicted by the IC/CMB model, poses important problems related to their extremely long radiative cooling time. In fact we know that the X–ray emission (as well as the optical and radio ones) comes from localized regions of the jet (knots), despite the fact that the X–ray emitting electrons cannot radiatively cool inside these volumes. This motivated the exploration of the possible effects of adiabatic losses that for low energy electrons can be much more efficient than radiative losses. In particular we have identified two possible scenarios: case A corresponds to standing shocks, while case B reproduces the situation of moving emitting blobs. Some general consequences relevant for future and more detailed observations will be briefly discussed below and in a forthcoming paper.

However, the existing observations already pose a problem. In fact the comparison of our results with the available data of the nearby aligned radio source (i.e. blazar) 3C 273, reveals that in either cases (A or B) radiative and adiabatic losses cannot explain what is observed. In case A one would expect radio (and perhaps X–ray) knots larger than the optical ones, contrary to observations. In case B unobserved "fossil knots", bright in the radio and especially in the X–ray band, but much fainter in the optical, should be detected.

A plausible alternative is that the emitting region is clumped. This allows the particles to cool by adiabatic expansion more efficiently than in the homogeneous knot case. Such clumps can originate from different processes. An important consequence of this scenario is that, at least in the simplest assumptions, the emitting region is far from equipartition, with the particle energy density dominating over the magnetic one.

6. Discussion

In large scale jets, characterized by moderate values of the magnetic and photon energy densities, the radiative cooling times can exceed the dynamical timescales for all but the TeV electrons responsible for the high energy tail of the synchrotron emission. In particular, in the IC/CMB models the X–ray flux is produced by electrons with random Lorentz factors of the order of 10–100, implying that they do not cool in a dynamical timescale through radiation losses. Adiabatic losses then play a crucial role to account for the knotty morphology of large scale X–ray/optical/radio jets. We envisaged and considered two scenarios for the dissipation and acceleration site: accelerated particles can be injected either at the front of a standing shock or throughout a blob moving along the jet.

In the first case we expect to observe the emission region extending downstream of the shock, with a size depending on the observing frequency. In particular, the X–ray emitting region should be larger than the radio one, as X–rays are produced by lower energy electrons. The predicted optical behavior is more complex, as the emission would be initially due to the highest energy and rapidly cooling electrons via synchrotron and later to the lowest energy electrons via IC.

In the case of a moving blob particles would be confined and evolve within the blob. The particle evolution then corresponds to a time dependent appearance of the blob itself. In such situation old/fossil blobs are expected to be observable particularly bright in the X–ray and relatively less in the radio and optical bands. In fact the lifetime of the X–ray emission is long (compared to the light crossing time of the blob) even taking into account adiabatic losses, and therefore the number of fossil blobs should be larger than that of those recently lightened up.

These considerations suggest the possibility of discriminating between the two scenarios: the observations of X–ray trails, more elongated than the radio and the optical ones, would favor the standing shock scenario, while the detection of isolated X–ray knots with weaker, but cospatial radio and optical emission, would argue for moving blobs.

Some indications can be already inferred from nearby blazars for which HST can probe the interesting spatial scales. We have compared our results with the existing data of 3C 273, which show a fast decrease of flux outside the knots and no detection of fossil knots. This evidence can be accounted for if knots are actually clumped, and the emission is the convolution from several small emission sites, as in this case particles can adiabatically cool within the observed knot and the flux outside it decreases fast.

A direct consequence of the clumping scenario is that the emission can be variable on short (months–years) timescales. Indeed recently the knot HST–1 in M 87 (emitting by synchrotron from the radio to the X–ray band) has been reported to vary by a factor two on a timescale of months in the X–ray and optical bands and not in the radio one (Harris et al. 2003). These variations have been attributed to the radiative cooling of the synchrotron emitting electrons. However, the dimension of knot HST–1 is of the order of ∼100 pc, implying through the causality argument, a minimum observable variability timescale of ∼300 years. If the HST–1 knot is instead composed of several clumps, the minimum variability timescale corresponds to the light crossing time of each clump (as long as the total number of clumps is not so large to dilute the variability amplitude below the detection limit). M 87, then, also shows some evidence for clumped substructure in the jet knots, as we have suggested in the case of 3C 273 using a completely independent argument.

More fundamentally, if the jet is actually a continuous fluid with concentrated acceleration sites and *cold* particles, perhaps embedded in a very low magnetic field, between knots, deeper observations should detect inter-knots inverse Compton emission due to the cold particle bulk motion (bulk Comptonization). Such emission would be concentrated in the IR-optical band, at $\sim 10^{14}$ Hz. This offers a powerful diagnostic of such medium in a near future with NGST. Clearly the possibility of detecting such emission mainly depends on the density of the medium: nevertheless even an upper limit could provide information on the density contrast between the knots and the inter-knot medium, the actual content of jets, their power, and the acceleration process. Thus observations of large scale emission with high sensitivity in different bands would provide an important piece of information for interpreting the emission and the corresponding physical conditions in large scale jets, but more importantly would constitute a powerful means for understanding the structure of extragalactic jets and whether they are formed and propagate as a continuous fluid or as episodic ejections of magnetized plasma, as might be the case for Galactic microquasars.

Acknowledgements. We thank Tomaso Belloni and Daniele Malesani for useful discussions and the anonymous referee for helpful criticism. The Italian MIUR and ASI are acknowledged for financial support.

References

Blandford, R. D., & Königl, A. 1979, ApJ, 232, 34
Celotti, A., Ghisellini, G., & Chiaberge, M. 2001, MNRAS, 321, L1
Chiaberge, M., & Ghisellini, G. 1999, MNRAS, 306, 551
Chartas, G., Worrall, D. M., Birkinshaw, M., et al. 2000, ApJ, 542, 655
Drenkhahn, G., & Spruit, H. C. 2002, A&A, 391, 1141

Ghisellini, G., & Celotti, A. 2001, MNRAS, 327, 739
Hardcastle, M. J., Worrall, D. M., Birkinshaw, M., Laing, R. A., & Bridle, A. H. 2002, MNRAS, 334, 182
Hardcastle, M. J., Birkinshaw, M., & Worrall, D. M. 2001, MNRAS, 326, 1499
Harris, D. E., & Krawczynski, H. 2002, ApJ, 565, 244
Harris, D. E., Biretta, J. A., Junor, W., et al. 2003, ApJ, 586, L41
Kraft, R. P., Forman, W. R., Jones, C., et al. 2002, ApJ, 569, 54
Marshall, H. L., Harris, D. E., Grimest, J. P., et al. 2001, ApJ, 549, L167
Pesce, J. E., Sambruna, R. M., Tavecchio, F., et al. 2001, ApJ, 556, L79
Sambruna, R. M., Maraschi, L., Tavecchio, F., et al. 2002, ApJ, 571, 206
Sambruna, R. M., Urry, C. M., Tavecchio, F., et al. 2001, ApJ, 549, L161
Schwartz, D. A. 2002, ApJ, 571, L71
Schwartz, D. A., Marshall, H. L., Lovell, J. E. J., et al. 2000, ApJ, 540, L69
Siemiginowska, A., Bechtold, J., Aldcroft, T. L., et al. 2002, ApJ, 570, 543
Sikora, M., Blazejowski, M., Begelman, M. C., & Moderski, R. 2001, ApJ, 554, 1
Tavecchio, F., Maraschi, L., Sambruna, R. M., & Urry, C. M. 2000, ApJ, 544, L23
Wilson, A. S., & Yang, Y. 2002, ApJ, 568, 133
Wilson, A. S., Young, A. J., & Shopbell, P. L. 2001, ApJ, 547, 740